Energy Reduction in Lithium-ion Battery Manufacturing using Heat Pumps and Heat Exchanger Networks

Håkon Guddingsmo* Petter Martinussen* Daniel Stjernen* Asanthi Jinasena Anders Hammer Strømman Odne Stokke Burheim

Department of Energy and Process Engineering, Norwegian University of Science and Technology, Norway,
{haakogud,pettma,daniestj}@stud.ntnu.no,
{asanthi.jinasena,anders.hammer.stromman,odne.s.burheim}@ntnu.no
* Equally contributed

Abstract

Global electric mobility is rapidly expanding. Hence, the demand for lithium-ion batteries is also increasing fast. Therefore, understanding energy minimization options in this rapidly growing industry is crucial for reducing the environmental impact as well as developing low-cost and sustainable batteries. The biggest contribution to greenhouse gas emissions is the cell manufacturing process. The most energy-intensive steps of cell manufacturing are electrode drying and dry room conditioning. Therefore, we developed process models for these two systems that can be used for evaluating various energy optimization techniques, such as heat pumps and heat exchanger networks. Further, various process options can be tested and benchmarked in terms of their overall energy consumption using these models. The results show that the power requirement may be reduced through all the options assessed, and available energy efficiency measures may substantially lower the energy footprint of cell production with strong relevance for subsequent greenhouse gas footprints.

Keywords: lithium-ion battery, energy optimization, electric vehicle, electrode drying, dry room, sustainable energy, pinch analysis, heat pump

1 Introduction

Today's transport sector is shifting from fossil-fueled vehicles to electric vehicles. Although this is currently a slow transition, the global market for electric vehicles is expected to grow rapidly in the future. The demand for lithium-ion batteries (LIB) for these vehicles is also expected to increase simultaneously. Having a low carbon footprint is a requirement for ensuring climate change mitigation with this growth. Life cycle assessment studies on battery electric vehicles have shown that the carbon footprint of LIB production may contribute to significant greenhouse gas emissions (Kurland, 2020; Ellingsen et al., 2016). One of the main drivers for these emissions is identified as the energy usage of the cell manufacturing process (Kurland, 2020). Although emissions vary over different regions, energy saving is always important.

Therefore, today's LIB research is advancing towards energy-efficient, low-cost, and sustainable cell manufacturing techniques. Adaption of less energy-intensive technologies such as advanced drying technologies (Bryntesen et al., 2021) or semisolid-state and solid-state battery manufacturing technologies is becoming popular in this regard. Identifying various energy minimization options for the conventional cell manufacturing process is equally crucial for today's battery industry.

The most energy-intensive steps of conventional cell manufacturing are electrode drying and dry room conditioning (Dai et al., 2019; Yuan et al., 2017; Jinasena et al., 2021). Energy for a convective cathode drying and a solvent recovery system is modeled by Ahmed et al. (2016b), while different dry room air conditioning systems using solid desiccant wheels are modeled by Vogt et al. (2021) and Ahmed et al. (2016a). Although these processes have been studied individually, and their energy impacts were analyzed in detail, there are no studies that explore the energy minimization options of the combined process. There are possibilities of applying a heat pump to facilitate exchanges between the electrode drying process and the dry room air conditioning system. In addition, the general use of heat exchanger networks to exchange various heating and cooling loads is also of interest.

Therefore, this study's main objective is to explore these two possibilities to minimize the total energy requirement of the energy-intensive process steps of LIB cell manufacturing. For this, we have developed process models for electrode drying and dry room air conditioning such that various process options can be tested and benchmarked in terms of their overall energy consumption.

2 System Description

A $LiNi_{1/3}Mn_{1/3}Co_{1/3}O_2$ (NMC111) cell production factory of 530 MWh annual capacity is selected for the study. Out of the cell production process, only the electrode drying process, solvent recovery system and the dry room air dehumidification system were considered for the study due to their high energy intensity. Different options of energy recovery is explored between these systems. The modeling approaches for each system is described in this section.

2.1 Electrode Drying

Conventionally, the drying is performed using convective heat transfer and high temperature air circulating over the electrode films. Alternatively, this can also be performed using radiation drying. Drying rate and drying time differ depending on solvent used and the temperature inside the chamber. To reduce the amount of energy consumed during drying, a multistage drying process can potentially be utilized. This alternative drying process can consist of splitting the drying chamber into multiple sections with different temperatures, ranging from low to high temperature drying. Alternatively, the temperature can be controlled in intervals when utilizing a batch dryer. This will reduce the overall heating load in comparison to a single-stage heating process, as it will reduce the amount of air that needs to be heated.

The electrode drying process is modeled using a reduced-order model for two different technologies, convection drying (CD) using hot air and infra-red radiation drying (RD) using radiation heaters (Oppegård et al., 2020). For more details on the model see Oppegård et al. (2020).

2.2 Solvent Recovery System

Water soluble N-Methyl-2-pyrrolidone (NMP) can be used as a solvent for the mixing of cathode material powders during LIB manufacturing. The need for recovering and recycling this solvent is prominent due to its polluting and hazardous nature. For this, an intricate filtration process is applied. A typical NMP recovery system is shown in Figure 1. Condensation is used in order to extract the NMP from the air exiting the drying stage. However, the complete solvent recovery system is not modeled in the study, where the solvent removal columns are omitted. The heat and mass transfer of the thermal units are modeled using Aspen Plus. Based on Ahmed et al. (2016b), the air needs to be cooled to approximately 6°C. The required cooling energy is assumed to be equal to that of the heating when considering conservation of energy.

Furthermore, this is mainly applicable to the cathode, as most of the anode material mixing are usually water-based. Due to the use of water as solvent, the anode is assumed to not require a solvent recovery process.

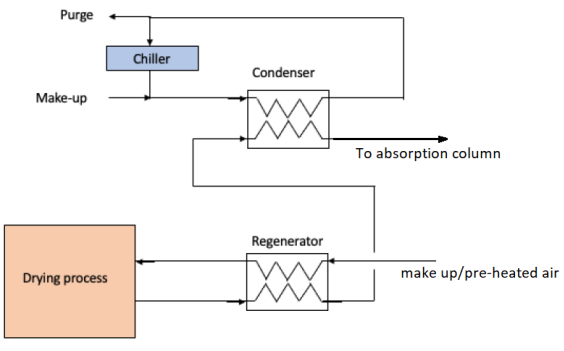

Figure 1. The NMP recovery system.

2.3 Dry Room Air Dehumidification System

A dry room is an enclosure with low humidity and a certain level of cleanness. It is an essential part for processes that require a dry and clean environment, such as the cell assembly stages in a battery manufacturing process. Liquid electrolyte filling is highly sensitive to water vapor. The dry air supply for the dry room can be obtained by an air dehumidification system. Common air dehumidifiers are mostly operated by either a solid desiccant wheel or a liquid desiccant system.

The liquid desiccant system is a mechanism that removes humidity and sensible heat from the air through the use of a liquid desiccant material and thermal energy. Calcium chloride ($CaCl_2$) is a commonly used desiccant for this purpose. Figure 2 depicts a basic configuration.

Here, the absorber and regenerator columns are connected through a piping system. The water in the humid air entering the absorber column is bound to the liquid desiccant, and the dried air then exit at the top of the same column. A heater increases the temperature of the water-filled desiccant to 100°C upon entry of the regenerative column. The water is then evaporated, while the residual desiccant is pumped into the absorber column while subsequently being cooled to 25°C, closing the loop. The heat and mass transfer of the complete system with an additional heater for dry air heating is modeled in Aspen Plus.

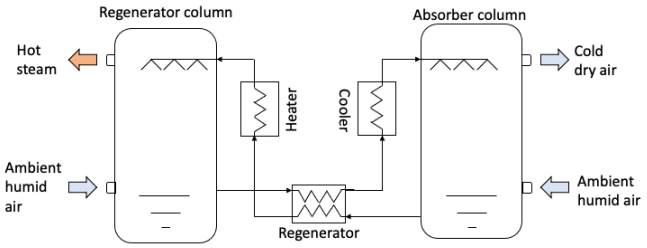

Figure 2. The liquid desiccant system.

2.4 Heat Pump

A heat pump is a system that transfers energy between two thermal reservoirs of different temperatures. The system is based on the vapor compression refrigeration cycle. A common configuration of a heat pump is shown in Figure 3 which consists of an evaporator, compressor, condenser and expansion valve. At the inlet of the evaporator (low temperature), the circulating fluid of the cycle is a vapor-liquid mixture. When passing through the evaporator, the liquid evaporates using the energy transferred from the cold reservoir. The fluid then enters the compressor, which increases the pressure of the fluid to become saturated vapor. The high temperature vapor then enters the condenser which absorbs energy by converting the fluid from vapor to saturated liquid. In this process, the energy is released in the form of heat, which is then transported into the hot reservoir. The fluid is then expanded adiabatically through an expansion valve which returns it to the

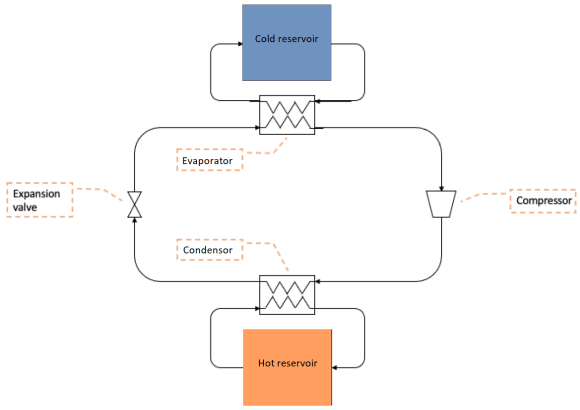

Figure 3. A typical heat pump configuration.

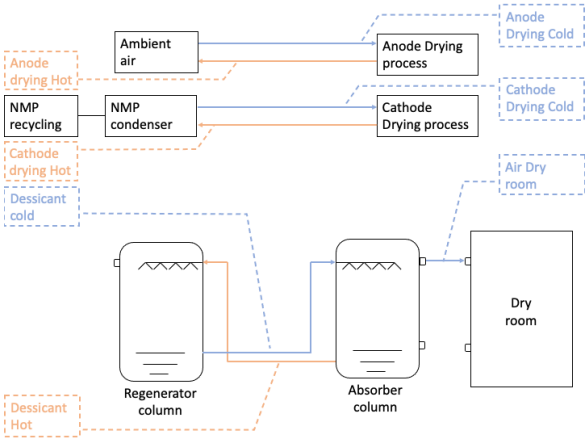

Figure 4. Streams evaluated using pinch approach.

same state as the evaporator inlet, closing the loop (Moran et al., 2018).

The heat pump is modeled in Aspen and various refrigerants were used as the working fluid of the heat pump based on the availability and thermodynamic characteristics. The refrigerants are R-22 (chlorodifluoromethane), R-134a (tetrafluoroethane) and R-600a (isobutane). Different condensation and evaporation temperature and pressure characteristics were also tested to find out the optimum operational conditions.

2.5 Heat Exchanger Networks

A Maximum Energy Recovery (MER) network is a system that is based on pinch analysis and consists of a network of heat exchangers optimally placed for maximum energy recovery within the system. A further option investigated utilizing different MER-network designs within the entire systems heat exchangers. These networks are designed using the heat exchanger details resulted from the models and the corresponding pinch analyses were performed. How the streams of the network are connected in the network configurations is depicted in Figure 4. This was the basis for simulation. The streams shown in the figure are categorized as hot and cold. The cold streams are in need of heating, while hot streams are in need of cooling. The figure also shows all the material streams involved in the production process. These streams consisted of three groups. The first of these being the anode streams, with both inlet and outlet from the drying process. Secondly, the cathode streams were connected between the drying process and the NMP recycling unit. Finally, the dry room streams consisted of the two streams within the desiccant system, between the absorber and regenerator column, as well as the airflow into the dry room. The streams presented here essentially represent the total system before any connections were made.

The minimum temperature difference was set to 10°C. Aspen Energy Analyser was used to design the MER-network, based on the input streams listed in Table 1. The number of stream splits allowed was set to zero, in order to simplify the design. The design yielded the energy requirements and heat exchanger sizes required for the design. A series of designs were produced connecting different heat exchangers based on the pinch approach. The simplicity of the connections and the total costs were considered during the design.

Table 1. The input values for the pinch analysis in Aspen Energy Analyser.

Stream	*Temperature range [°C]*	*Mass flow rate [kg/h]*	*Heat cap. [kJ/kgK]*
Desiccant hot	78–25	2 000	3.71
Desiccant cold	6–100	2 000	3.71
Air dry room	5–23	32 000	1.00
Cathode hot	140–6	34 200	1.00
Cathode cold	6–140	34 200	1.00
Anode hot	140–8	34 200	1.00
Anode cold	8–140	34 200	1.00

3 Results and Discussion

3.1 Effect of Parameters on the Evaporation Energy of Drying

For the drying process, the evaporation energy and drying time are heavily impacted by the parameters of the air entering the convective dryer, with temperature, velocity and humidity being the prominent factors.

Figure 5 shows the effect of these parameters on the power requirement for the evaporation of solvent and Figure 6 shows the effect on the evaporation energy for one batch of NMC111 cathode production. Parameters were changed one at a time and all the parameters were normalized for illustration. The process parameters have a significant effect on the evaporation energy in both CD and RD. However, in comparison to the other energy values in the cell production process, the evaporation energy is insignificant (less than 0.2 Wh/Wh) which makes the variations of process parameters less significant for evaporation energy consumption. It is important to note that although

faster drying rates can be achieved with high temperatures, drying rate is controlled to prevent binder migration and cracking of electrodes (Jaiser et al., 2016; Rollag et al., 2019; Westphal et al., 2015). Therefore, multi-stage drying is preferred (Oppegård et al., 2020).

The initial conditions are selected according to the battery chemistry specifics and the heat source temperature is taken as 140°C. For an NMC111 cathode, the CD time and evaporation power is 19.2 minutes and 28.7 kW, respectively. For a graphite anode, the CD time is 13.7 minutes and the power needed for evaporation becomes 41.9 kW. Thus, the load needed for evaporation using CD is collectively 70.6 kW for a NMC111-based cell.

Similarly, the power and energy requirements are calculated for RD, resulting in 40.9 kW (0.089 Wh/Wh) for cathode and 58.2 kW (0.086 Wh/Wh) for anode, respectively (see Figure 7). For both anode and cathode drying, RD is faster than CD due to faster drying rates towards the end of the drying process. The drying time has a significant effect on the power requirement as the power is higher for RD than CD. However, the total energy requirement can be considered similar between CD and RD as the change in values is comparatively low (0.003 Wh/Wh).

3.2 Effect of Drying Temperature and Regenerator Size on the Energy of Solvent Recovery System

The solvent recovery system was tested for different drying temperatures of 80°C and 140°C (for CD), as well as for various heat exchanger sizes. Table 2 shows the heating and cooling loads for the cathode drying system when operating at these temperatures. The total load is for the heating of the anode, and the heating and cooling of the cathode. The regenerator is an additional heat exchanger to the system shown in Figure 1 to be used in the heat pump and for further energy recovery. Regenerator load zero represents the original solvent recovery system without additional energy recovery.

Through the implementation of a regenerative unit, the decrease in required power is shown to be linear for the heating and cooling loads. When the regenerator size is bigger with higher load, the total heat exchanger load is lower than the original system, which shows that more energy can be recovered by the regenerator. Lowering the dryer air temperature also show a significant impact on the power requirement. However, as discussed in Section 3.1, the decrease in temperature results in a increase in drying time, which would affect the production capacity and the energy consumption per cell.

For anode drying, it is assumed that the anode utilizes water as solvent instead of NMP, and does not require a solvent recovery process. This removes the need for cooling. However, a regenerative unit can still be implemented for the anode air stream. The anode heating load would be equal to the cathode heating load of 1208 kW and 707

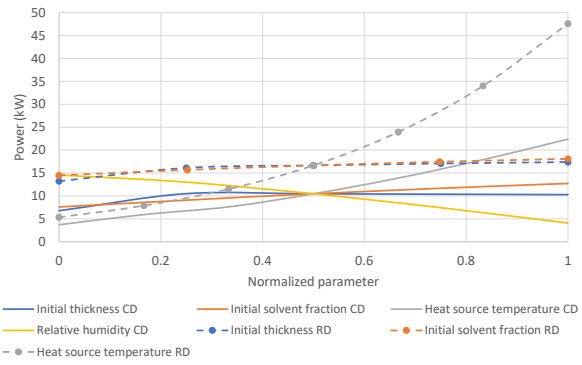

Figure 5. Effect of initial and operating conditions on the power requirement for evaporation by convection and radiation.

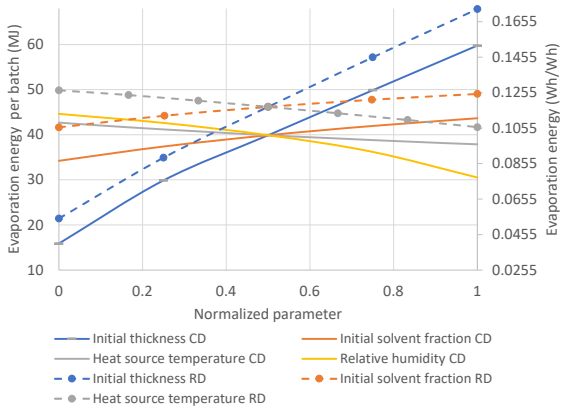

Figure 6. Effect of initial and operating conditions on the evaporation energy by convection and radiation.

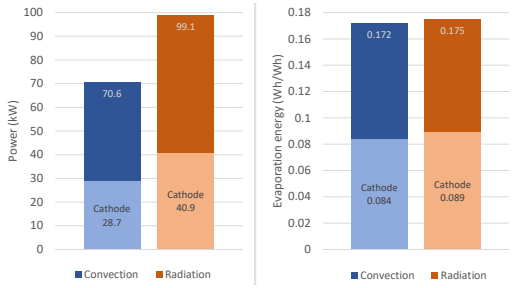

Figure 7. Power and energy requirements for evaporation of anode and cathode solvents by convection and radiation.

Table 2. The heat exchanger loads with various regenerator sizes for a 80°C and 140°C CD process.

Temperature (°C)	*Regenerator [kW]*	*Heating [kW]*	*Cooling [kW]*	*Total [kW]*
80	0	663	663	1989
	100	563	563	1689
	250	412	412	1236
	500	163	163	489
140	0	1208	1208	3624
	100	1108	1108	3324
	250	958	958	2874
	500	707	707	2121

kW for 140°C, without and with a 500 kW regenerator, respectively.

For both cathode and anode drying the total load amounts to 3624 kW for the original system at 140°C and 2121 kW with two 500 kW regenerators (one for each drying process). Similarly, for RD, the heating load for cathode drying is taken as 742 kW, where the required heating and cooling loads without regeneration amounts to a total of 2226 kW.

3.3 Energy Consumption with Heat Pump

The heat pump that is applied between the drying system and the dehumidification system is shown in Figure 8. The different regenerator sizes tested in Section 3.2 are used here. The selected refrigerants were also tested, which yielded different pressure ranges for the condenser and evaporator of the heat pump. Further, the required compressor energy was found for the desired operating conditions of the heat pump. It is observed that the lower pressure ranges have a higher required compressor power for the heat pump to be able to operate under ideal conditions.

The heat pump design is highly based on the characteristics of the attached systems. For example, for a dry room heater load of 132.1 kW, the heat pump requires a regenerator duty of 1090 kW or alternatively an additional heat exchanger connected to the desiccant system to assist in cooling the stream.

Therefore, using a heat pump requires a large sized regenerator, since the heating load for the desiccant system is selected as 150 kW. This would require a regenerator duty of 940 kW. The resulting temperature ranges of the streams connected to the heat pump would be 20–6°C for the electrode drying stream and 8–23°C for the dry room air flow. The temperature difference is too small to use a regular heat exchanger and using a heat pump is therefore viable.

Table 3 displays the compressor power, pressure ranges and coefficient of performance of the compressor based on tested refrigerants. R–600a is selected as the refrigerant for the study due to the lower pressure range. The heat pump in this proposed design covers the entire heating load for air entering the dry room as well as contributing to cooling the air stream for NMP extraction. The potential power savings are considered as 247.9 kW, although, this is highly dependent on the refrigerant used.

Table 3. The pressure ranges and compressor power requirement for different refrigerants in the heat pump. COP: coefficient of performance

Refrigerant	*Pressure (bar)*	*Compressor power (kW)*	*COP factor*
R–22	4.37–12.67	9.3	14.10
R–134a	2.53–8.25	16.2	8.17
R–600a	1.37–4.33	20.1	6.58

3.4 Energy Consumption with MER-Network

The composite curve and the grand composite curve for the system is shown in Figure 9. The composite curve is parallel showing a high possibility of energy recovery. A clear pinch point is also seen at 10°C. According to the grand composite curve there is an energy pocket up to 150 kW, which indicates excess energy that cannot be used for a heat exchanger due to the available low temperature range. However, theoretically, this allows a heat pump to be operated based on the temperature ranges that were analyzed for the operation of heat pump in section 3.3. Therefore, implementing a heat pump in combination with a MER-network has the potential to theoretically save around 300 kW, including both heating and cooling.

Three MER networks (named MER-1, MER-2 and MER-3) were designed and one of the designed MER-networks (MER-1) are shown in Figure 10. The blue horizontal lines of the network represent the cold streams and the orange horizontal lines represent the hot streams in the total system. The heat exchanger connections are indicated by the vertical connection lines between the streams, where blue dots indicate the coolers connected to the cold utility stream (refrigerant/cooling water), orange dots indicate the heaters connected to the hot utility stream (steam/hot water), while the gray dots indicate the regenerators interconnected to process streams. The minimum temperature difference for the pinch analysis is taken as 10°C for all the designs.

For MER-1 and 2, the utility streams were chosen arbi-

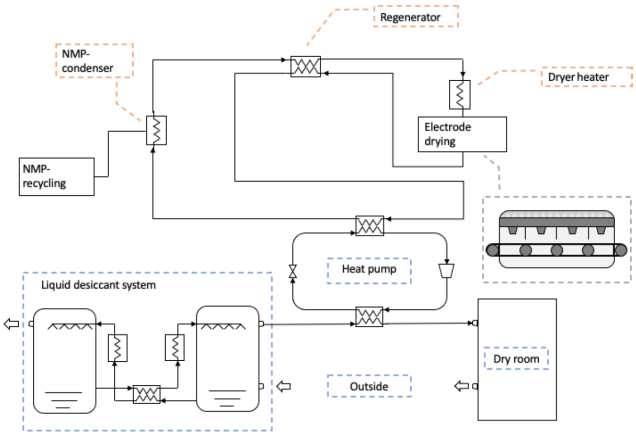

Figure 8. Applied heat pump configuration.

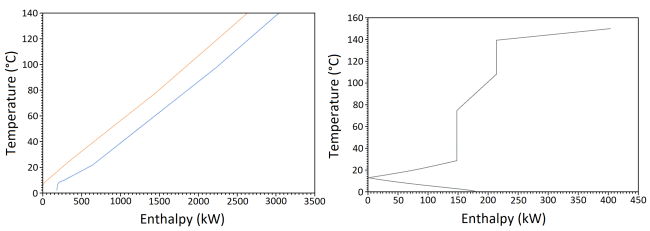

Figure 9. The composite and grand composite curves.

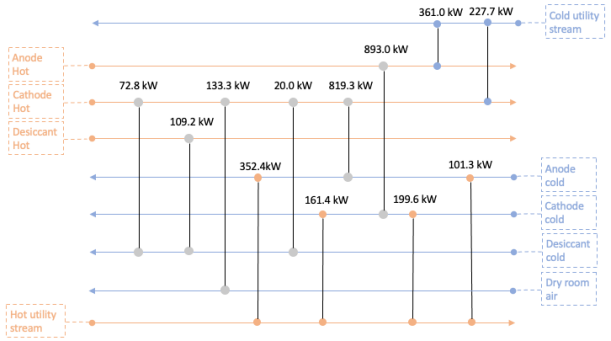

Figure 10. MER-network design one (MER-1).

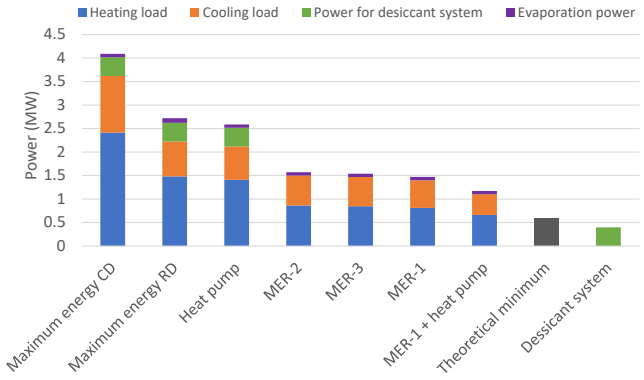

Figure 11. A comparison of power requirements with different energy reduction methods including a heat pump and MER heat exchanger network designs.

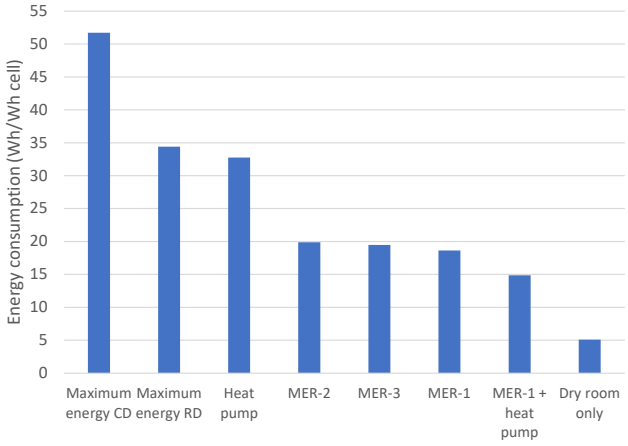

Figure 12. The energy consumption for different energy optimization methods.

trarily since it does not impact the energy demand. However, this impacts the required area of the heat exchangers representing cooling and heating units, which directly affects the capital cost which is not considered in the study. MER-1 network consists of twelve heat exchangers, where four of them are heaters and two are coolers. The total heating and cooling requirements for this design are 814.7 kW and 588.7 kW, respectively, and 1403.4 kW in total. The largest regenerator in this design needs a heat exchanger area of 775 m^2 and the total area for heat exchangers is 2058 m^2.

Similarly, for MER-2, thirteen heat exchangers are used including four heaters and two coolers. The power requirement for this design is 864.7 kW for heating and 638.6 kW for cooling which gives a total power of 1503.3 kW. This is a slightly higher power requirement than the first design. The largest heat exchanger in this design is of an area of 900 m^2 and the total area for heat exchangers is 1825 m^2.

The third design, MER-3 was done using four heaters, three coolers and five regenerators. The power requirement for this design is similar to MER-1 with a total of 1471.2 kW, where 848.7 kW for heating and 622.5 kW for cooling, respectively. In MER-3, the largest heat exchanger is 697 m^2 with a total heat exchanger area of 1928 m^2.

All the network designs have two remaining low temperature coolers at the top right and a low temperature heating load to the bottom left in the respective designs. There is a potential for connecting a heat exchanger between these two heating and cooling loads which can further reduce the total power requirement of all three designs.

3.5 Comparison of the Used Energy Optimization Methods

Total power requirement from all the assessed methods are compared together as shown in Figure 11. The total system without any energy recovery is used as the maximum power requirement for the system either with a convective (4090 kW or 51.7 Wh/Wh) or radiation (2720 kW or 34.3 Wh/Wh) drying process. The system with RD is lower in energy, about 17.3 Wh/Wh (1370 kW) compared to the CD system. The energy recovery methods are applied only to the system with CD.

The addition of a regenerator in the solvent recovery system, and the heat pump between the regenerator and desiccant system heater, has decreased the power requirements by 1503 kW (19 Wh/Wh). The MER-network designs have reduced the power requirements further down by 2620 kW (33.1 Wh/Wh), 2520 kW (31.8 Wh/Wh) and 2552 kW (32.2 Wh/Wh) for MER-1, MER-2 and MER-3, respectively. The difference of each network is by approximately 100 kW between each other. By implementing a heat pump together with the MER-1 design, the total power is further decreased by 300 kW (3.8 Wh/Wh). A theoretical minimum power requirement (581 kW) for the MER-networks is also included as a comparison followed by the power requirement for the dry room dehumidification system which can be compared with production processes without drying, such as semi-solid-state batteries.

The energy requirements for the same optimization methods are calculated with respect to the produced cell capacity for NMC111 cell production. The total energy consumption values are shown in Figure 12 for the se-

lected energy saving options. A similar reduction of energy trend can be seen from the figure.

The results suggest that the energy requirement can be reduced through all the options assessed. In total, the results indicate a potential for substantial improvements in overall energy intensity for the production of different battery chemistries (energy usage in Wh per Wh of produced battery) when heat exchanger networks are used for heat recovery. This can be further enhanced by combining the heat exchanger networks with the heat pumps. In summary, this work suggests that available energy efficiency measures may substantially lower the energy footprint of LIB production with strong relevance for subsequent greenhouse gas footprints.

3.6 Comparison with Literature Values

The energy values for the range of various energy optimization methods are compared together with the energy values reported in literature. The MWh to GWh scale plant data reported by Yuan et al. (2017), Pettinger and Dong (2017), Schünemann (2015), Dai et al. (2019), and Sun et al. (2020) are considered here. Further, the models developed by Ahmed et al. (2016a,b) and Jinasena et al. (2021) are also included in the comparison. The compared values for dry room and drying energy consumption are shown in Figure 13.

The values are not comparable with their variation due to the different plant capacities. However, the values for dry room and drying with MER-networks are well comparable with similar capacity values of a 0.7 GWh plant data by Schünemann (2015, cited in Thomitzek et al., 2019). The values of this study are slightly higher than the values from Schünemann (2015, cited in Thomitzek et al., 2019), which could be due to the slightly lower plant capacity of this study.

Ahmed et al. (2016b) investigated the energy for cathode drying and solvent recovery process for an annual plant capacity of 1 GWh. For their base case of a CD process of 37 m^3/s air flow, the power for the electrode dryer is 130 kW, where in our study the maximum power (out of various initial drying conditions) is 26 kW for a flow of 7.5 m^3/s cathode dryer air flow. The total power for their process is given as 5851 kW (42.1 Wh/Wh pack) where 1470 kW of electrical power and 4381 kW of thermal power. This amount (42.1 Wh/Wh) is the second highest energy requirement out of the reported values, where the highest is 51.2 Wh/Wh for a 18.2 MWh plant reported by (Yuan et al., 2017). Further, this value is only for the cathode drying which suggest the energy values will be higher for both cathode and anode drying. The plant consists of a fuel fired air heater of 3752 kW, a chiller of 1169 kW (electricity), and a condenser of 3508 kW which is connected to an air-to-air heat exchanger for energy recovery (2700 kW). The total electric power for air blowers is 301 kW. Additionally, there is a 236 kW re-heater for the regeneration air of the desiccant wheel, and a 394 kW heater for the distillation column where the recovered NMP is further purified for reuse. The total power requirement in their study for various process parameters is in the range of 3346–7304 kW (24.1–52.6 Wh/Wh). In our study we haven't included the blowers or the NMP purification column which gives a slightly underestimated value for the energy requirement.

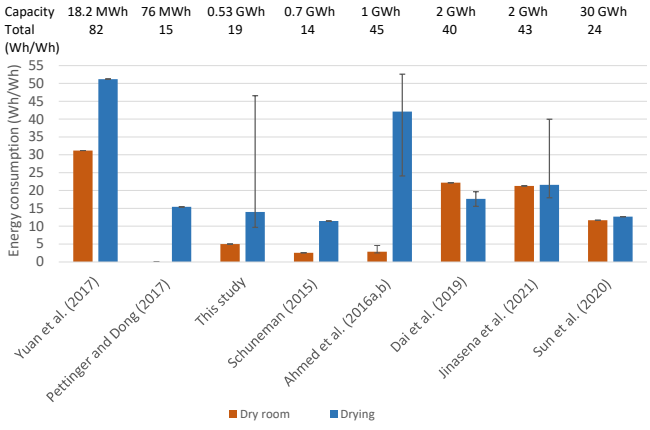

Figure 13. The comparison of energy consumption values for drying and dry room with reported literature values. The average total energy and the annual capacity of each production facility are also stated.

Similarly, Ahmed et al. (2016a) modeled a 16 000 m^3 dry room for a dry air flow of 20 m^3/s. The system uses a zeolite wheel for moisture removal, and consists of a cooler (426 kW), pre-cooler (57 kW), heater (63 kW), regenerator (30 kW) and blowers (167 kW). For a base case of operating conditions the total power was determined as 398 kW. Assuming that they produced 10 kWh battery packs (similar to Ahmed et al. (2016b)) this value is around 2.9 Wh/Wh which is comparatively low.

Further, Thomitzek et al. (2019) reported a 133.6 Wh/Wh for drying and 448.7 Wh/Wh for dry room for a 48 kWh annual capacity pilot plant. For this plant, Vogt et al. (2021) report a total power of 271.8 kW for a dry room which supplies 2.74 m^3/s dry air flow. This includes two pre-coolers of 54.8 kW and 43.8 kW, a process fan of 15 kW, a re-heater of 33.2 kW, and a regeneration heater of 125 kW with a 15 kW heat recovery.

These results show that comparing the values of different scales is difficult because of the high variance of the reported values. Therefore, the models need to be scaled up or redesigned for giga factory scale for a proper comparison. Vogt et al. (2021) have reported scaling-up of their pilot scale energy data. They report a reduction of energy consumption of the dry room from 20.98 kWh per cell (Wessel et al., 2021) to 1.45 kWh per cell. However, this is equivalent to approximately 47 Wh/Wh and is still higher than the other reported values. Therefore, scaling-up of smaller scale plant data and models, and development of giga scale plant models need to be further explored for accurate energy consumption estimations for battery industry.

4 Conclusions

Process models were developed for a dry room air conditioning system and electrode drying processes of a lithium-ion battery production process, for analyzing different energy optimization options. For the drying process, different drying techniques were explored, namely convection air drying and infra-red radiation drying. The energy consumption for radiation drying is lower than for convection drying without any energy recovery in the convection process. Application of a heat pump and use of maximum energy recovery heat exchanger network design based on pinch analysis are explored as energy optimization techniques. For the system with convection drying, a heat pump reduced the energy usage considerably. Application of heat exchanger networks reduced the energy usage more than the heat pump. The combination of both these techniques resulted in the most energy reduction for the total process system from 51.7 Wh/Wh to 14.9 Wh/Wh.

Acknowledgement

We acknowledge Freyr Battery AS (grant 02-2019-IP172-FREYR) for the funding of the study.

References

Shabbir Ahmed, Paul A. Nelson, and Dennis W. Dees. Study of a dry room in a battery manufacturing plant using a process model. *Journal of Power Sources*, 326:490–497, 2016a. doi:10.1016/j.jpowsour.2016.06.107.

Shabbir Ahmed, Paul A. Nelson, Kevin G. Gallagher, and Dennis W. Dees. Energy impact of cathode drying and solvent recovery during lithium-ion battery manufacturing. *Journal of Power Sources*, 322:169–178, 2016b. doi:10.1016/j.jpowsour.2016.04.102.

Silje Bryntesen, Anders Strømman, Ignat Tolstorebrov, Paul Shearing, Jacob Lamb, and Odne Burheim. Opportunities for the State-of-the-Art Production of LIB Electrodes—A Review. *Energies*, 14:1406, 2021. doi:10.3390/en14051406.

Qiang Dai, Jarod C. Kelly, Linda Gaines, and Michael Wang. Life cycle analysis of lithium-ion batteries for automotive applications. *Batteries*, 5(48), 2019. doi:10.3390/batteries5020048.

Linda Ellingsen, Bhawna Singh, and Anders H. Strømman. The size and range effect:Life-cycle greenhouse gas emissions of electric vehicles. *Environmental Research Letters*, 11:1–9, 2016.

Stefan Jaiser, Marcus Müller, Michael Baunach, Werner Bauer, Philip Scharfer, and Wilhelm Schabel. Investigation of film solidification and binder migration during drying of li-ion battery anodes. *Journal of Power Sources*, 318:210–219, 2016. doi:https://doi.org/10.1016/j.jpowsour.2016.04.018.

Asanthi Jinasena, Odne S. Burheim, and Anders H. Strømman. A Flexible Model for Benchmarking the Energy Usage of Automotive Lithium-Ion Battery Cell Manufacturing. *Batteries*, 7(1):14, 2021. doi:10.3390/batteries7010014.

Simon Davidsson Kurland. Energy use for GWh-scale lithium-ion battery production. *Environmental Research Communications*, 2(1):012001, 2020. doi:10.1088/2515-7620/ab5e1e.

Michael J. Moran, Howard N. Shapiro, Daisie D. Boettner, and Margaret B. Bailey. *Fundamentals of Engineering Thermodynamics*. Wiley, 9th edition, 2018. ISBN 978-1-119-39138-8.

Emil Oppegård, Asanthi Jinasena, Anders H. Strømman, Jon A. Suul, and Odne S. Burheim. Study of an Industrial Electrode Dryer of a Lithium-Ion Battery Manufacturing Plant: Dynamic Modelling. In *61st Conference on Simulation and Modelling*, pages 77–84, Virtual, 2020. doi:10.3384/ecp2017677.

Karl Heinz Pettinger and Winny Dong. When does the operation of a battery become environmentally positive? *Journal of the Electrochemical Society*, 164(1):A6274–A6277, 2017. ISSN 19457111. doi:10.1149/2.0401701jes.

Kelsey Rollag, Daniel Juarez-Robles, Zhijia Du, David L. Wood, and Partha P. Mukherjee. Drying Temperature and Capillarity-Driven Crack Formation in Aqueous Processing of Li-Ion Battery Electrodes. *ACS Applied Energy Materials*, 2(6):4464–4476, 2019. doi:10.1021/acsaem.9b00704.

Jan-Hinnerk Schünemann. *Modell zur Bewertung der Herstellkosten von Lithiumionenbatteriezellen*. Sierke, 1st edition, 2015. ISBN 978-3-86844-704-0.

Xin Sun, Xiaoli Luo, Zhan Zhang, Fanran Meng, and Jianxin Yang. Life cycle assessment of lithium nickel cobalt manganese oxide (NCM) batteries for electric passenger vehicles. *Journal of Cleaner Production*, 273:123006, 2020. ISSN 09596526. doi:10.1016/j.jclepro.2020.123006.

Matthias Thomitzek, Nicolas Von Drachenfels, Felipe Cerdas, Christoph Herrmann, and Sebastian Thiede. Simulation-based assessment of the energy demand in battery cell manufacturing. *Procedia CIRP*, 80:126–131, 2019. ISSN 22128271. doi:10.1016/j.procir.2019.01.097.

Marcus Vogt, Klemens Koch, Artem Turetskyy, Felipe Cerdas, Sebastian Thiede, and Christoph Herrmann. Model-based energy analysis of a dry room HVAC system in battery cell production. *Procedia CIRP*, 98:157–162, 2021. doi:10.1016/j.procir.2021.01.023.

Jacob Wessel, Artem Turetskyy, Felipe Cerdas, and Christoph Herrmann. Integrated Material-Energy-Quality Assessment for Lithium-ion Battery Cell Manufacturing. *Procedia CIRP*, 98:388–393, 2021. ISSN 22128271. doi:10.1016/j.procir.2021.01.122.

Bastian Westphal, Henrike Bockholt, T. Gunther, W. Haselrieder, and Arno Kwade. Influence of convective drying parameters on electrode performance and physical electrode properties. *ECS Transactions*, 64(22):57–68, 2015. doi:10.1149/06422.0057ecst.

Chris Yuan, Yelin Deng, Tonghui Li, and Fan Yang. Manufacturing energy analysis of lithium ion battery pack for electric vehicles. *CIRP Annals - Manufacturing Technology*, 66(1): 53–56, 2017. doi:10.1016/j.cirp.2017.04.109.